Construction and Building Materials 403 (2023) 133055

Contents lists available at ScienceDirect

Construction and Building Materials

journal homepage: www.elsevier.com/locate/conbuildmat

Damage evaluation and mechanisms of textile reinforced concrete during telescopic failure

V.J.F. Alexandre [a], W.P. Boshoff [b], R. Combrinck [a,*]

[a] University of Stellenbosch, South Africa
[b] University of Pretoria, South Africa

ARTICLE INFO

Keywords:
Textile reinforced concrete (TRC)
Pull-out
Failure mechanisms
Mechanical properties

ABSTRACT

Textile-reinforced concrete (TRC) offers a solution to the drawback associated with the production of cement and its use in construction. It also promotes the design of concrete in a post-cracking stage as the yarns bridge cracks once the concrete fails in tension. The pull-out behaviour of TRC has and still receives considerable attention to progress its use, but the full extent and types of mechanisms associated with the pull-out is not yet fully understood. This research sets out to investigate the pull-out mechanism when considering various embedment lengths, as well as employing the use of X-ray computed tomography and scanning electronic microscope imaging on the post-pull-out elements. The study identified a bottleneck mechanism, resulting from the undulating imprint the warp yarn produces, which improves the pull-out resistance of yarns. Additionally, the latter mentioned mechanism is also enhanced by the effect of congestion caused by filament debris, resulting from the telescopic failure.

1. Introduction

Textile-reinforced concrete (TRC) is a composite fabricated by embedding technical textiles in a cement-based matrix (CBM). The textiles are typically made from non-corrosive filaments referred to as a yarn, which in turn may comprise one single macro filament or made from a series of multi-filaments. Two sets of yarns are laid orthogonally to form a grid-like structure and are termed the weft and warp yarns as shown in Fig. 1. Generally, the textile has high tensile strength and when used in conjunction with the CBM, which has a low tensile threshold, can create a composite with favourable mechanical properties [1–5] and provides a solution to durability related topics [6–8].

Strain-hardening can be achieved in TRC when the volume percentage of a textile of adequate strength is sufficient. This behaviour can be demarked to have three distinct stages based on the Aveston-Cooper-Kelly (ACK) model, as shown in Fig. 2 [9,10].

Stage I is the region in which the TRC exhibits an elastic-linear behaviour. The end of this stage is denoted by the occurrence of the first crack within the matrix and the onset of Stage II. Stage II can be divided into two subsections: Stage IIa and Stage IIb. Stage IIa denotes the formation of new cracks across the matrix as the applied load increases and ends when no new cracks are formed. The latter is referred to as the crack saturation point. Stage IIb is defined as the point after crack saturation and encompasses the crack-widening process of pre-existing cracks as the load intensity increases. The end of Stage IIb is marked by the failure of the composite, as the commonly used technical textiles have no plastic capacity and Stage III is typically not reached for TRC.

Textiles composed of multi-filament yarns have a variation in the stress distribution across the yarn cross-section when the filaments are not impregnated by an epoxy. This variation results in the yarn not behaving as a cohesive unit when loaded. Instead, the yarn can be described to be presented as a series of concentric filament layers, as shown in Fig. 3. Three layers can be distinguished: (i) the sleeve filaments that are in direct contact with the matrix, (ii) the intermediate filaments that are in contact with both filaments and the matrix, and (iii) the core filaments that are only in contact with other filaments. The sleeve layer is stressed to a higher degree as loading commences due to the higher degree of friction and starts rupturing before the remaining layers. The successive rupturing causes the forces to be transferred to the subsequent intact layer. At the same time, the intermediate and core filaments start slipping as the cracks widen but at greater ease due to the reduced frictional resistance. That is to say that the inner filaments can slip out at a lower applied force. This process of systematic slipping of

* Corresponding author.
E-mail addresses: vital@burmeister.com.na (V.J.F. Alexandre), billy.boshoff@up.ac.za (W.P. Boshoff), rcom@sun.ac.za (R. Combrinck).

https://doi.org/10.1016/j.conbuildmat.2023.133055
Received 7 December 2022; Received in revised form 31 July 2023; Accepted 18 August 2023
Available online 1 September 2023

the layers is referred to as telescopic failure [12].

The bonding mechanism and behaviour between the textile and the concrete matrix have gained attention in numerous studies as it does influence the nature of the TRC failure modes [13–28].

Understanding the global behaviour of TRC composites is essential and can be achieved by outlining and understanding the factors and mechanisms that play a role in the bond between the textile and matrix. Signorini *et al.* [28] found that uncoated specimens do not reach the full potential of reinforced textiles and that the mechanical performance is greatly insensitive to the type of textile. Additionally, the aforementioned provides information on creating and improving models used to predict TRC behaviour [20,29–31].

Factors that influence bonding have been highlighted to include, but not limited to: the use of supplementary cementitious materials [12,32] and fillers [33–35], production process [20,36,37], textile geometry [38–40], textile type [19,40,41], and the use of coatings [42–49]. An additional factor affecting bonding also originates from the presence of weft yarns [12,50–53].

Jiang *et al.* [23] studied the effect of embedment length and textile geometry on bonding behaviour. Their study concluded that the shear stress decreases with an increase in embedment length and that an optimal mesh spacing exists for uniform textile mesh impregnation. Furthermore, three failure modes were identified: pull-out, textile rupture, and a combined failure. Williams Portal *et al.* [6] reports the same failure modes yet state that the failure is dependent not only on the length but also on the type of textile used. For example, carbon-based textiles failed by slipping in all instances, but basalt bases textiles varied between slipping and rupturing.

Coating, such as styrene butadiene, enhances the bond properties [44–46]. Scheffler *et al.* [54] report that adding a coating influences the interphase, between the filaments and the matrix, by increasing the stiffness. Moreover, the former mention states that coatings also affect the load transfer between the textile and the matrix. The application of styrene butadiene does not compare, in terms of performance, to epoxy impregnation. The former results in lower stiffness and this, in turn, leads to the formation of a wider crack spacing [55]. Similarly, Zhu *et al.* [48], found that the addition of an expoxy improves the stiffness of a TRC sample during the first stage of the pull-out process due to the improved bond.

Generally, the studies conducted focus on the coatings and type of material the textile consist of. Similarly, the post-pull-out behaviour is generally limited to the extracted yarns to deduce what mechanisms are at play. However, studies of focussing on single fibre pull-out of steel fibres have yielded interesting results when employing CT-scanning methods on the post-pull out test specimens, including the matrices

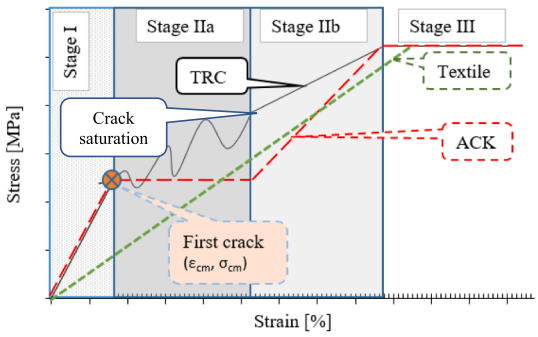

Fig. 2. Typical mechanical response of TRC during static loading (redrawn from [11]).

[56,57]. Extending these methods to TRC specimens could also prove valuable in providing insights into the factors that add to the increasing bond and pull-out resistance of yarns.

This study aims to add to the knowledge of the mechanisms involved in the telescopic failure of textiles when used as a constituent of TRC. This in turn can provide information relating to more consistent and comprehensive design approaches. This work focuses on the damage evaluation of a yarn during and after it has been pulled out and how it relates to the mechanisms attributed to the damage. Alkali-resistant (AR) glass textiles are used in studies due to its low cost in comparison to other textiles, such as carbon-based textiles. This study considers the behaviour of AR glass textiles when being pulled out and the damage mechanisms by evaluating the extracted yarns and the matrix it is extracted from.

2. Experimental programme

2.1. Materials

This study used an alkali-resistant (AR) glass textile in union with a CBM. Each filament of the yarn is coated with a styrene butadiene layer that gives the textile resistance against the alkaline concrete environment during the curing process before testing [58]. However, during testing the styrene butadiene layer might be damaged, exposing the glass filaments to chemical deterioration. The impact of the deterioration is considered to be negligible due to the short duration of exposure during the quasi-static tests (less than 15 min) conducted in this study [59,60]. The impact of the deterioration on the pull-out behaviour is likely to be more significant for long-term tests, such as creep testing,

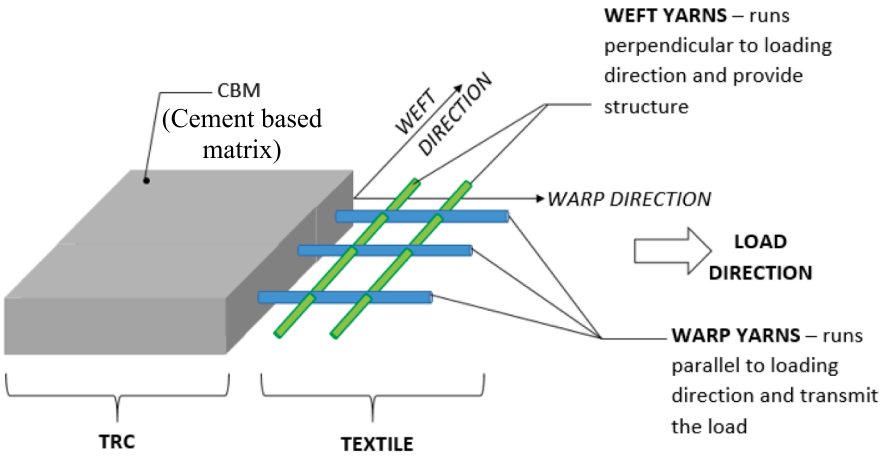

Fig. 1. The levels and components of a typical textile-reinforced concrete (TRC).

which does not form part of this article [61,62]. Fig. 4 illustrates the mesh size of the textile (23 × 23 mm^2) and a typical cross-section of the warp and weft yarns. The physical and mechanical properties of the textile are provided in Table 1 as per the supplier's specifications [63]. The diameter provided in Table 1 is the equivalent diameter of the yarns represented by a circular cross-section with an equal area.

The constituents and proportions of the mentioned CBM are given in Table 2. The constituents for the concrete matrix were all locally sourced. The cementitious components consisted of a CEM II/A-L (52.5 N) cement, a class F fly ash, and silica fume. The only aggregate used in the mix was a natural quarry sand locally referred to as Malmesbury sand. The maximum particle size of the fine aggregate was limited to 2.36 mm. The grading of the sand is illustrated in Fig. 5. A high-range water-reducing super-plasticiser, Dynamon SP1 as supplied by Mapei [64], was incorporated into the mix to achieve a mix with good workability and plastic consistency. The average compressive strength of the matrix at 28 days, taken as the average of seven 100 mm cubes, is 53.3 MPa (standard deviation of 1.9 MPa).

2.2. Specimen preparation

Pull-out test samples were cast in wooden moulds with dimensions of 500 × 80 × 12 mm. The moulds are oiled and filled with the mixture to half the volumetric capacity and vibrated briefly for 5–10 s, using a table vibrator set to a low level, even though the mixture has a relatively good flowability (average slump flow of 234 mm). Hereafter, a single layer of the textile measuring 500 mm in length and 80 mm in width was laid down by hand and slightly pressed to ensure good contact between the matrix and the entire textile's bottom surface. The mould was then filled with the matrix and vibrated lightly for 5–10 s. These specimens were demoulded after 24 h and placed in water curing tanks at 23 °C for a further 27 days.

At an age of 28 days after casting, the specimens were cut in half to produce two samples measuring 250 × 80 × 12 mm, based on the recommendations set out by [65]. The cut sections also aided in identifying and confirming the location of the warp yarns. After identifying the locations of the warp yarns, two holes were drilled along the central line of the specimen at predetermined locations where the central yarn of the textile was located. The upper hole (H1), shown in Fig. 6, was used as a connection duct for the experimental set-up discussed in the next section (Section 3.3).

The second/lower hole (H2) was introduced to ensure that the warp yarn was disconnected at the required location for the required embedment length being tested. As measured from H2 as shown in Figure 4.6, a distance equal to the embedment length marked the location for notching the concrete sample. The notch was made to ensure that only one warp yarn is being tested during the loading process, i.e. that only the central warp yarn is effectively continuous and taking part during the pull-out procedure. This sample preparation allows for the double-sided pull-out test as described next [66,67].

2.3. Pull-out tests

There currently exists no standardised test exists for pulling-out tests for single yarn in CBM. However, there are two ways of performing pull-out tests, namely, (i) a single-sided pull-out test (SSPOT) [13] and (ii) a double-sided pull-out test (DSPOT) [66,67]. For this study, the DSPOT test was chosen and a discussion on the benefits and shortcomings of the tests can be found elsewhere [6].

The set-up used in this study for the DSPOT is shown in Fig. 7. The tests were performed using a Zwick Z250 universal testing machine. The upper clamp of the machine secured a connection plate connected to a 50 kN load cell. The upper section of the samples is connected to the load cell using a pin connection at H1, ensuring that no clamping pressure is imposed on the upper portion of the matrix containing the shorter yarn portion. The cross-head displacement was recorded, but two additional 50 mm spring-loaded linear variable differential transducers (LVDT) were introduced to compare the yarn's actual displacement. The lower half of the specimen was gripped by the pneumatic clamps of the test machine at the same position (the bottom 100 mm length) for each specimen.

Care was also taken not to damage the matrix connecting the two sections at the notched section. Achieving this proved problematic as the area and level of reinforcing was low and therefore susceptible to being easily damaged.

Five embedment lengths were chosen for investigation: 25, 30, 40, 50, and 60 mm. The test was controlled by the cross-head displacement at a rate of 1 mm/min. The notation used to distinguish the samples is denoted as S-(*embedment length*)-(*sample number*). For example, S25-1 would represent Sample 1 at an embedment length of 25 mm.

2.4. Imaging

The post-pull-out damage was investigated using macro-X-ray computed tomography (CT) imaging and a scanning electron microscope (SEM). A prismatic section of the matrix surrounding the yarn was procured by cutting out a 10 × 10 mm section along the embedment length, as shown by the highlighted portion in Fig. 6 for post-pull-out analysis. These cut-outs were only done for the upper section of the matrix that contained the shorter end of the yarn being pulled out. These sections are, in turn, x-rayed and the results analysed. The yarns that were pulled out were also analysed using a SEM to assess the damage on the yarn after it has been pulled out.

3. Results and discussion

This study aimed to investigate the bonding mechanism of yarns in TRC on a single yarn level. The AR-glass textile was embedded at different lengths to determine if the failure mode was affected by this difference and the impact that the weft yarns might have with the subsequent increase in embedment length. All the points of interest for the experiments are given in Table 3. The stress is calculated by dividing

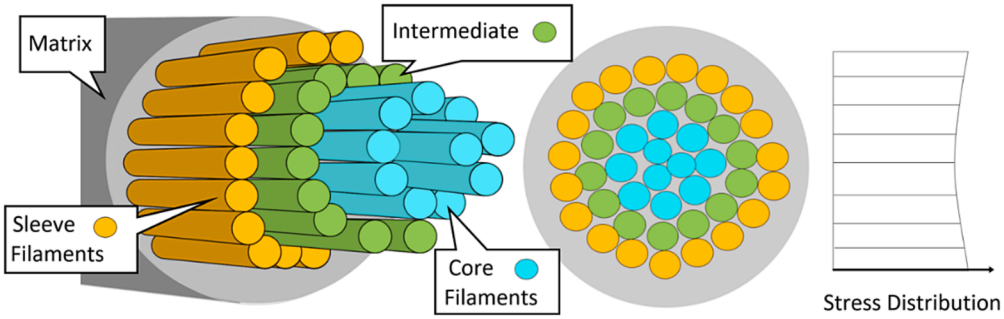

Fig. 3. Typical depiction of the telescopic nature of technical textiles and the stress distribution.

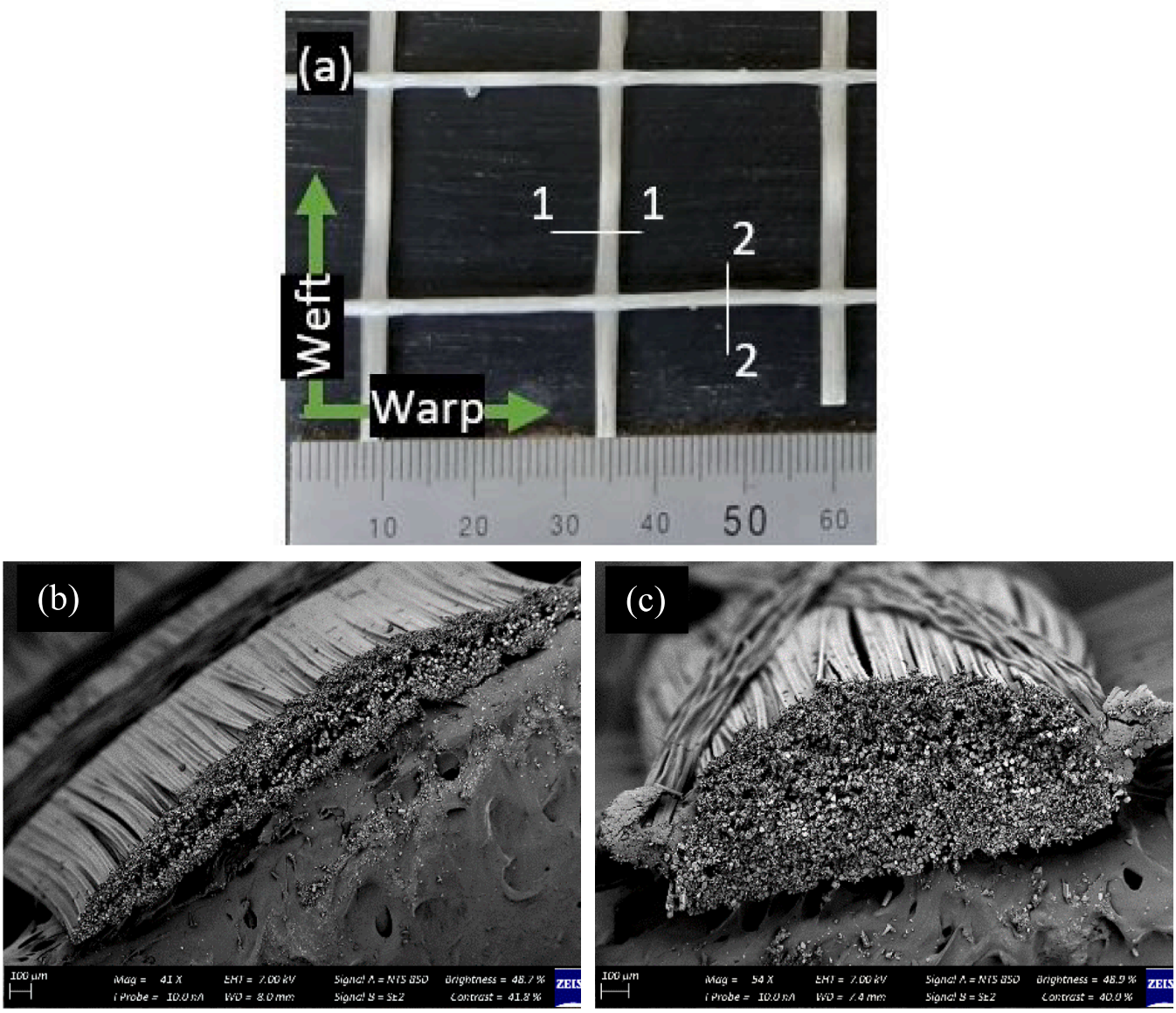

Fig. 4. AR-glass textile: (a) mesh size (values in mm), (b) Section 1-1: weft yarn -, and (c) Section 2–2: warp yarn cross-section.

Table 1
Mechanical and physical properties of the AR-Glass [63].

	Equivalent Diameter [mm]	Tensile Strength [MPa]	Filament Size [μm]	Tex Size [g/km]	Specific Gravity [g/cm^3]
Warp	0.75	1200	18–20	1200	2.68
Weft	0.75	1200	18–20	1200	2.68

the load by the cross-sectional area of an equivalent fictive yarn with a 0.75 mm diameter. The utility ratio, in turn, is determined as the ratio of the peak stress to the theoretical tensile capacity of the yarn, as given in Table 1.

Figs. 8 to 16 depict the results of the DSPOT for the various embedment lengths and the failure of a select few samples, chosen at random, to illustrate the different failure modes. Fig. 8 shows an excerpt of the embedment length where the matrix must be damaged before the yarn transmits the load. Due to the nature of the experimental set-up, the matrix at the vicinity of the notch for most of the samples had cracked while being handled and therefore they lacked the pronounced peaks

Table 2
Constituents and mix proportions of the matrix.

Constituent		Description	Relative Density (RD)	Quantity [kg/m^3]
Cementitious Binders	*Cement*	CEM II/A-L 52.5 N supplied by PPC.	3.14	438.0
	Fly Ash	Class F as supplied by Durapozz.	2.20	196.5
	Silica Fume	Microfine silica as supplied by Silicon Smelters.	2.21	22.5
Aggregate	*Sand*	A locally available natural quarry sand which has been sieved to allow a maximum particle size of 2.36 mm and a fineness modulus (FM) of 1.35.	2.56	804.0
Super-plasticiser		Dynamon SP1 as supplied by Mapei [64].	1.05	3.3
Water		Municipal tap water.	1.00	217.5

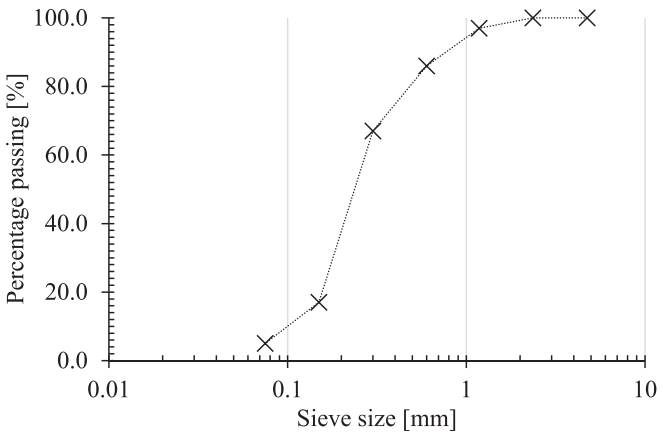

Fig. 5. The grading curve of the fine aggregate.

displayed in the aforementioned excerpt. Thus, only Fig. 8 depicts the excerpt. Also, the dashed lines, denoted with an additional prefix of W*x*, shown in the Figs. 8 to 16 denotes the location of the weft thread in relation to the extraction point.

Initially, the average pull-out force (P_{Max}) values decrease as the embedment length increases from 25 mm to 30 mm by 14.4 %. Nevertheless, there is an ensuing increase in the pull-out force as the embedment length increases from 30 mm to 40 mm and 50 mm by 38.7 % and 61.2 %, respectively. This increase can be explained by the increase in the contact area between the yarn and the matrix as the embedment length increases: the greater the contact surface area, the greater the frictional and bonding force required to be overcome. At 60 mm of embedment length, the failure mode transition to rupturing and the pull-out force decreases by 7.6 %. The failure mode is reported to be telescopic for the shorter embedment lengths, as shown in Figs. 9 and 11.

The location of the weft yarns (W1 and W2) in relation to the extraction point, as shown in Fig. 17, is also indicated in the respective figures. The tested TRC specimens were cut parallel to the warp yarn to establish the location of the weft yarns in relation to the notch, as shown in Fig. 17. As previously mentioned, the same notation is used for the load-slip curves in Figures 4.8, 4.10, 4.12, 4.13 and 15. However, an additional suffix is added, and it must be noted that this is merely the distance of the weft yarn from the extraction point. The suffix W1 therefore refers to the first weft yarn and W2 refers to the second weft yarn as measured from the extraction point, as shown in Fig. 17.

Table 3 provides a sense of variation of the primary peak loads which decreases with increasing embedment length. The variance is also reflected in the pull-out responses (Figs. 8, 10, 12, 13, and 15). The former mentioned is likely due to defects which cannot easily be avoided. The decrease in the variation is also attributed to the increased frictional resistance associated with the greater embedded lengths. In other words, the level extent of the defects may be less significant with the increasing resistance.

The variation at shorter anchorage lengths is also increased by samples which have primary peaks, which is the first peak achieved during the pull-out process, which is lower than the average. For example, S25-4 has a primary peak of 97.4 N, which is 73.3 N lower than the average and 173.9 N lower than the highest recorded primary peak (S25-2). Similarly, S30-2 recorded a peak of 61.2 N which is 71 N and 137.8 N lower than the average and maximum (S30-3) recorded primary peaks, respectively. The variation of these two samples can be because of an array of factors, or the compounding effect of these factors. Some of the causes of the reduced resistance can be the increased number of defects, air pockets which reduce the frictional resistance, human error,

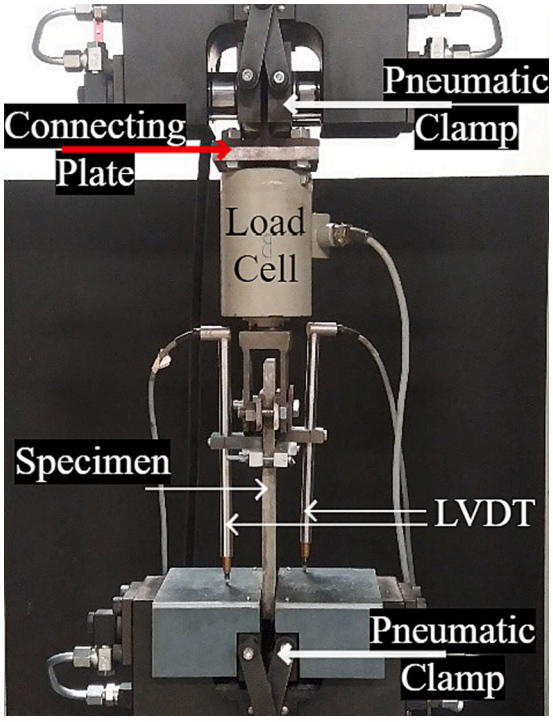

Fig. 7. Test set-up for the double-sided single yarn pull-out test.

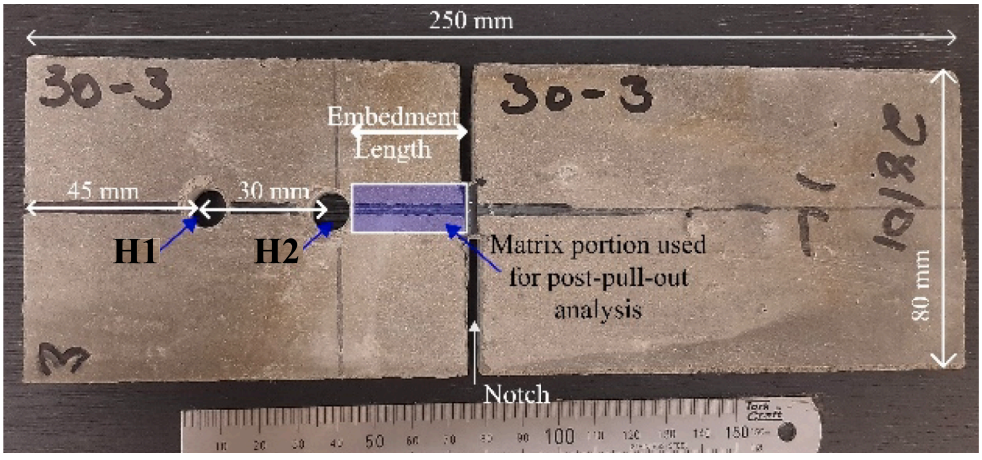

Fig. 6. Example of the specimen used for the pull-out tests.

Table 3
The pull-out test results.

Specimen	Length [mm]	Primary Peak Load [N]	Stress [MPa]	Utility Ratio [%]	Failure Mode
S25-1	25	183.7	415.8	34.7	Pull-out
S25-2	25	271.3	614.1	51.2	Pull-out
S25-3	25	156.1	353.3	29.4	Pull-out
S25-4	25	97.4	220.5	18.4	Pull-out
S25-5	25	142.0	321.4	26.8	Pull-out
S25-6	25	173.5	392.7	32.7	Pull-out
Average		170.7	386.4	32.2	
Standard Deviation		57.8 (33.9)*			
S30-1	30	144.1	326.2	27.2	Pull-out
S30-2	30	61.2	138.5	11.5	Pull-out
S30-3	30	199.0	450.4	37.5	Pull-out
S30-4	30	121.2	274.3	22.9	Pull-out
S30-5	30	112.3	214.2	21.2	Pull-out
S30-6	30	115.2	260.8	21.7	Pull-out
Average		132.2	299.2	24.9	
Standard Deviation		46.2 (35.0)*			
S40-1	40	232.6	526.5	43.9	Telescopic
S40-2	40	155.6	352.2	29.4	Telescopic
S40-3	40	151.8	343.6	28.6	Telescopic
Average		183.3	414.9	34.6	
Standard Deviation		35.3 (19.3)*			
S50-1	50	261.5	591.9	49.3	Telescopic
S50-2	50	299.7	678.3	56.5	Telescopic
S50-3	50	325.4	736.6	61.4	Telescopic
Average		295.5	668.9	55.7	
Standard Deviation		32.2 (10.9)*			
S60-1	60	295.2	668.2	55.7	Rupture
S60-2	60	279.8	633.3	52.8	Rupture
S60-3	60	243.3	550.7	45.9	Rupture
Average		272.8	617.5	51.5	
Standard Deviation		26.7 (9.8)*			

*The coefficient of variation (CoV) is given within the parenthesis.

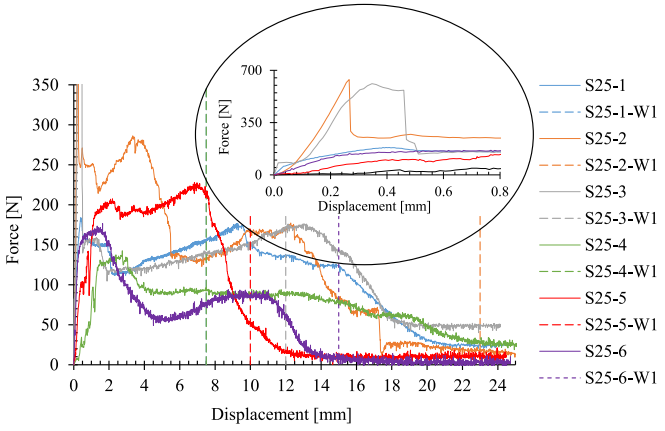

Fig. 8. The force versus displacement plot of double-sided pull-out for the 25 mm embedment with an insert of the truncated section.

yarn alignment, and test inadequacies [68].

The following section provides an in-depth discussion of the results. The discussion involves the pull-out behaviour, microstructural characterisations, and textile geometry.

3.1. Pull-out results behaviour

The results for the pull-out behaviour, as shown in Figs. 8 to 16, can be idealised as shown in Fig. 18. Three stages can be identified from this generalised behaviour model.

Firstly, a nearly linear response (Stage I) of the load-slip curve represents a perfect and elastic bond between the yarn and the matrix. In this instance, all the filaments are presumed to be intact. Hereafter, the response progresses to be non-linear (Stage II), indicating the debonding phase until the maximum load, P_{Max}, is reached. During Stage II, filament ruptures also occur [34,69]. Also, no slippage of the end section of the embedded yarn has yet occurred. The subsequent rupturing and reduction in the frictional resistance cause the load to drop. Stage III now represents the dynamic stage; strain-softening or strain-hardening develops depending on the mechanisms at hand. The latter mentioned occurring due to the frictional resistance of the fibre exceeding that of the maximum pull-out force (P_{Max}), and the former when the converse is true.

Strain-hardening is noted to be the primary response at the 25 and 30 mm embedment lengths (Figs. 8 and 10), which can be classified as the shorter embedment lengths. Strain-softening defines the pull-out response at longer embedment lengths, i.e. 40, 50 and 60 mm (Figs. 12, 13 and 15).

The aforementioned behaviour of the dynamic (slipping) stage, namely Stage III, can be justified by the effect of the telescopic behaviour of the textile. At shorter embedment lengths, the debonding takes place and the core and majority of the sleeve components pull out, as seen in the post-pull-out images of the 25 and 30 mm samples shown in Figs. 8 and 10. The sleeve is primarily intact due to the filament capacity not being reached. Valeri *et al.* [70] reported similar results and stated that the resistance of the yarn is related to the anchorage length.

For a longer embedment depth (40 and 50 mm), telescopic failure occurs as the sleeve filaments rupture (Stage III). There is a successive decrease in the circumferential area due to the sleeve filaments rupturing and disconnecting which leads to the core elements being the only element resisting the pull-out. Simultaneously, the core filaments are also reported to slip at a lower frictional surface, reducing the frictional resistance [12]. Fig. 14 shows the reduction in the yarn radius as a result of telescopic failure at longer embedment depths. However, Valeri *et al.* [70] do state that a certain level of slip is also required before the bond is activated. The former is noted in the strain hardening behaviour of the yarns with longer embedment which represents the second peaks forming as noted in the results of Figs. 12, 13, and 15.

When the embedment length increases to 60 mm, the third stage, i.e. Stage 3, is reduced to rupturing. The ductility of the pull-out curve is near absent for this series. The lack in the pull-out phase is likely due to the increase in circumferential area and embedment depth. This increase in the circumferential area increases the frictional resistance provided by the sleeve, resulting in rupturing to be the dominant failure mechanism for the 60 mm embedment length.

Additionally, the behaviour noticed in Stage III of the load-slip curve can be explained as a collective interaction of the following mechanisms: (i) the presence of fly ash and silica fume in the matrix composition, (ii) the straightening of the filaments, (training effect), and (iii) the interaction between the warp and weft yarns. These factors form the bases for the discussion of the following sections.

3.2. Microstructural characteristics

Figs. 9, 11, 14 and 16 shows the yarns of all embedment lengths post-pull-out. In these figures, the effect of telescopic failure is noticeable, especially with longer embedment lengths (40, 50, and 60 mm). Furthermore, Fig. 19 shows SEM images of the 25 mm versus 50 mm embedment lengths and further corroborates the evidence of the telescopic mechanism occurring. For instance, Fig. 19 (a) and (b) show the presence of ruptured filaments near the extraction point and halfway along the length of the specimen. These ruptured filaments are most likely located in the sleeve sections and it is also clear that more rupturing is present for the longer embedment lengths.

Fig. 19 (c) images display the end or tip of the extracted yarn after

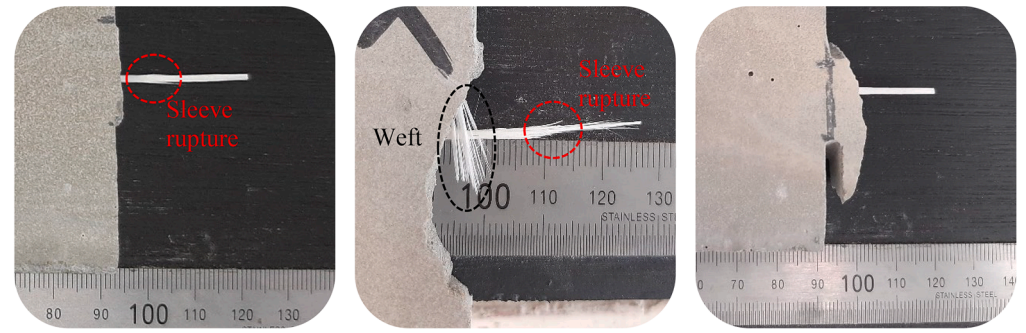

Fig. 9. Typical failure for the S25-series.

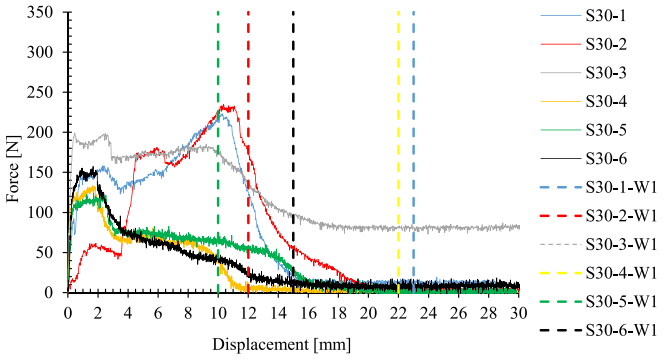

Fig. 10. The force versus displacement plot of double-sided pull-out for the 30 mm embedment.

being pulled out and can be presumed to represent the core section of the extracted yarn. The latter-mentioned images still indicate signs of ruptured filaments and relative slipping for the extracted yarn with a shorter embedded length (S25-1). The presumed core section of the yarns embedded at a longer depth (S50-1) has a reduced diameter and fewer ruptured filaments present, which is indicative of this portion being more inclined to slip out, as seen with the pull-out vs displacement curves (Figs. 8, 10, 12, 13, 15, and 18). Moreover, the thinner core portion has a reduced pull-out capacity due to the lower frictional resistance.

3.3. Presence of finer particles

The presence of finer particles, which include hydration products and silica fume, is suggested to increase the frictional resistance during pull-out [13,71]. Peled *et al.* [12] reports that adding fly ash in a CBM increased the pull-out force compared to a control mixture with no supplementary binders. The results in this study, particularly the presence of multiple peaks, are similar to those published by the authors as mentioned earlier.

Although the current study does not primarily focus on the influence of the matrix composition, it is worth mentioning that it does influence the pull-out resistance by affecting the interphase bond. Fig. 20 shows a typical case where smaller products can be seen to have penetrated a

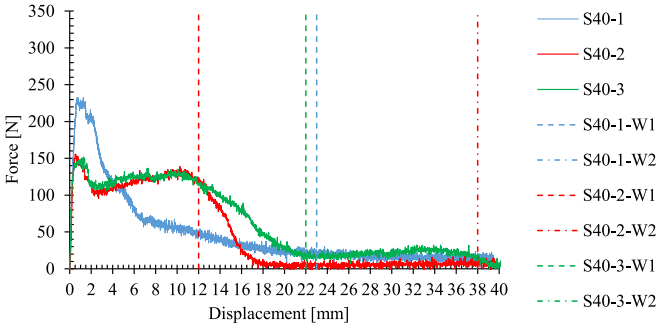

Fig. 12. The force versus displacement plot of double-sided pull-out for the 40 mm embedment.

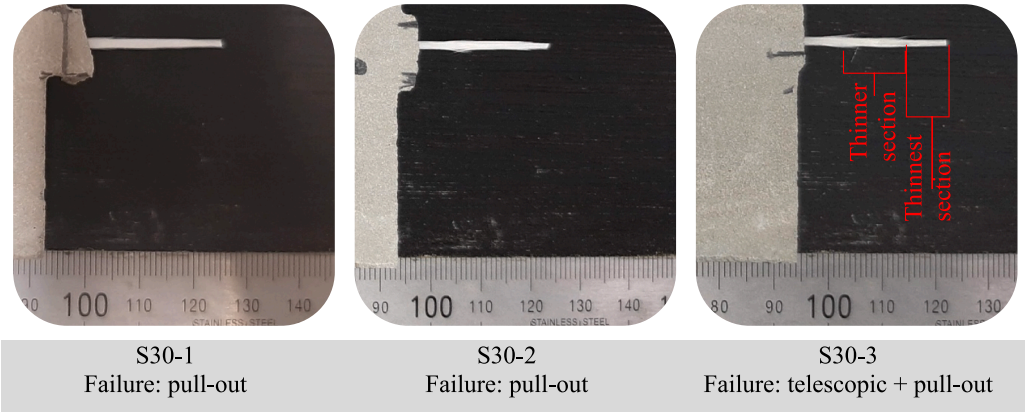

Fig. 11. Typical failure for the S30-series.

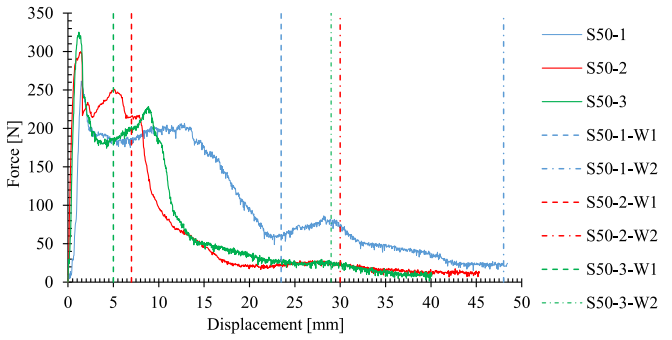

Fig. 13. The force versus displacement plot of double-sided pull-out for the 50 mm embedment.

yarn that has been pulled out. Upon closer inspection, S25-3 shown in Fig. 20, shows patches where the matrix has penetrated the yarn. These areas are also observed to contain fractured filaments, possibly due to the increased friction at these locations.

3.4. Slack

Individual filaments also have a certain degree of slack within the yarn and studies have shown that pre-stressing enhances the bond performance and therefore the mechanical performance of TRC [16,17,36,37,72]. Textiles may be pre-stressed during the production process of TRC to reduce the initial slack in the filaments. The TRC specimens for the current study were created using the hand-lay method. Hence, the filaments may be considered to have a certain degree of slack within it before being tested. The undulating pattern seen in the load-slip curves of Figs. 8, 10, 12, 13 and 15 can be explained to a degree by the straightening effect of the embedded textile. As these filaments start to become tauter, the strain within the filaments increases. The increase in strain causes an increase in the pull-out resistance, resulting in secondary peaks of the force versus displacement curves.

3.5. The presence of weft yarns

3.5.1. Mechanical interlock and geometry

The junction points of the warp and weft yarns are reported to contribute to the pull-out resistance [18,23,73]. A mechanical interlock is said to be generated by the presence of the weft yarn, as illustrated in Fig. 21 [12,50–53,74].

The presence of weft yarns also affects the geometry of a yarn within the textile. The periodic presence of weft yarns induces a crimping effect on the warp yarns which is mentioned to have a more significant impact than the anchoring mechanism shown in Fig. 21. The textile used in this study was also detected to have the geometry of the warp yarn affected along its length, as shown in Fig. 22. There is an apparent narrowing near the warp-weft junction due to the yarn stitching. The material packing of the warp yarn does increase further away from the junction due to the stitching and decreases again further away from the yarn junction. This variation in the thickness generates a bottlenecking effect closer to the intersection.

3.5.2. Bottleneck congestion

Fig. 23 to 25 depict the effect of the bottlenecking and geometry of the yarn junction on the pull-out of the warp yarn. These images are generated from the X-ray CT-scans of the sections that contained the embedded warp yarn (Fig. 6). These images indicate a congestion of warp yarn filament fragments accumulating near the bottlenecking junctions and are marked on the images.

It can be seen in Fig. 23 that there is a bundling of yarns on the side of the junction furthest from the extraction point, that is to say, at a location post-junction. This is corroborated by the images shown Fig. 24, displaying the cross-sectional view in the vicinity of the yarn junction, both ante- and post-junction. Ante-junction refers to the side of the intersection closer to the extraction point and post-junction is the side further away from the junction being investigated. For instance, Fig. 24 (a) indicates a section ante-junction where no weft yarn is present and minor warp filament fragments are noticed. Fig. 24 (b) – (c) shows how the accumulating fraction of warp yarn filament fragments increase at the location of a weft-warp yarn node, moving from the ante- to the post-junction, increases.

The same effect, where filament fragments cause congestion near the weft-warp yarn junction, is also seen in the specimens with a longer embedment depths. Fig. 25 (a) – (c) shows the progressive nature of the duct left in the matrix by the warp yarn and the accumulation of warp

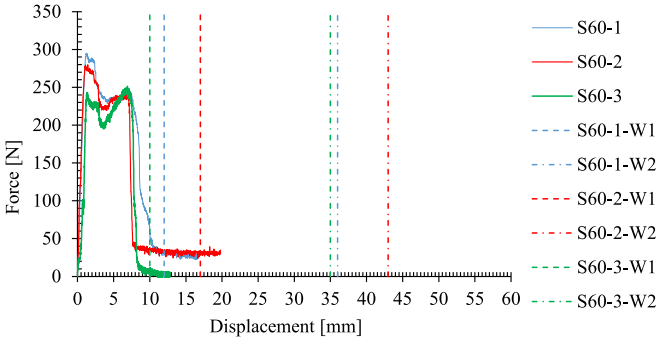

Fig. 15. The force versus displacement plot of double-sided pull-out for the 60 mm embedment.

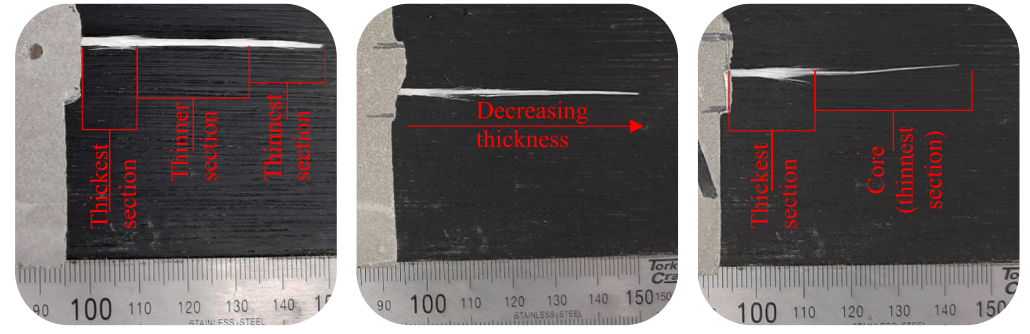

Fig. 14. Typical failure for the S50-series.

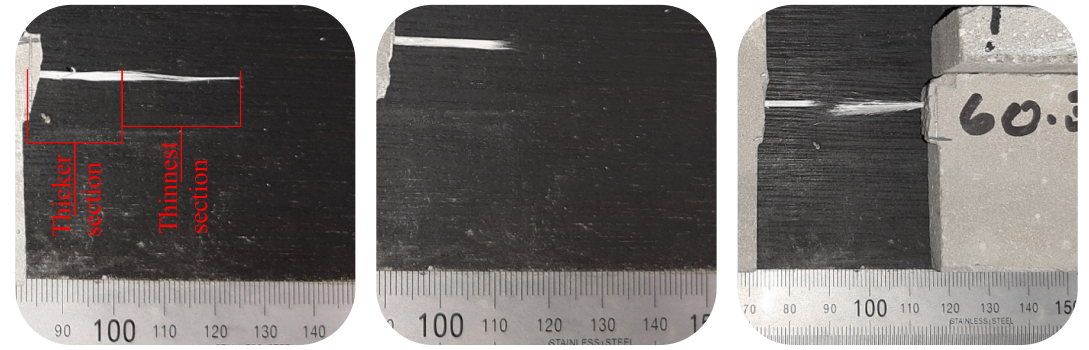

Fig. 16. Typical failure for the S60-series.

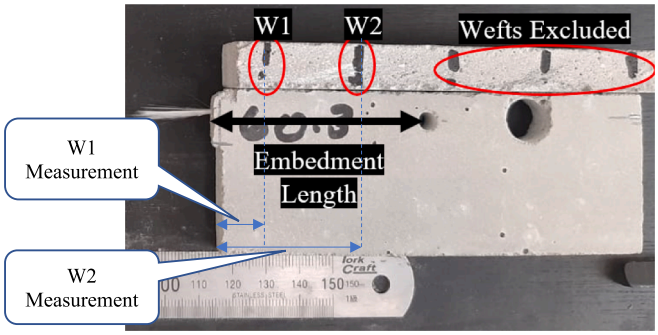

Fig. 17. A section cut through the matrix to identify the location of the weft yarn in relation to the notch.

yarn fragments in the duct at the post-junction location. In addition, Fig. 25 (d) shows the impact of the presence of a secondary junction on the bottlenecking and fragment conglomeration. The second junction shows a greater portion of warp yarn fragments compared to the first junction.

The congestion of the filament fragments has the beneficial effect of increasing the resistance of the yarn during the pull-out process. During the debonding process, filaments rupture during the loading process and start pulling out. As the pull-out process continues, the filaments are guided through the duct left by the warp yarn during the casting process and go through regions that may be narrower in certain sections than others. In more limited regions, the packing density of the filaments increases and there is an increase in the inter-filament friction, which creates resistance. Moreover, the debris of ruptured filaments also creates blockages in the ducts, adding to the aforementioned packing scenario, especially near the yarn junction. The increasing material congregating in the ducts therefore intensifies the frictional resistance. Thus, the stresses in the filaments increase at the weft-warp intersections and can cause additional filament rupturing while also increasing the resistance. Fig. 26 shows the damage on extracted yarns with damage visible and the associated resistance using the load–displacement graph at the respective levels.

In a study by Preinstorfer and Kollegger [75], the impact of bottlenecking is declared to have a minor impact on the bond behaviour between the textile and mortar. However, the study as mentioned earlier, focussed on a fully impregnated carbon-based textile. The aforementioned congested bottleneck mechanism is likely to be

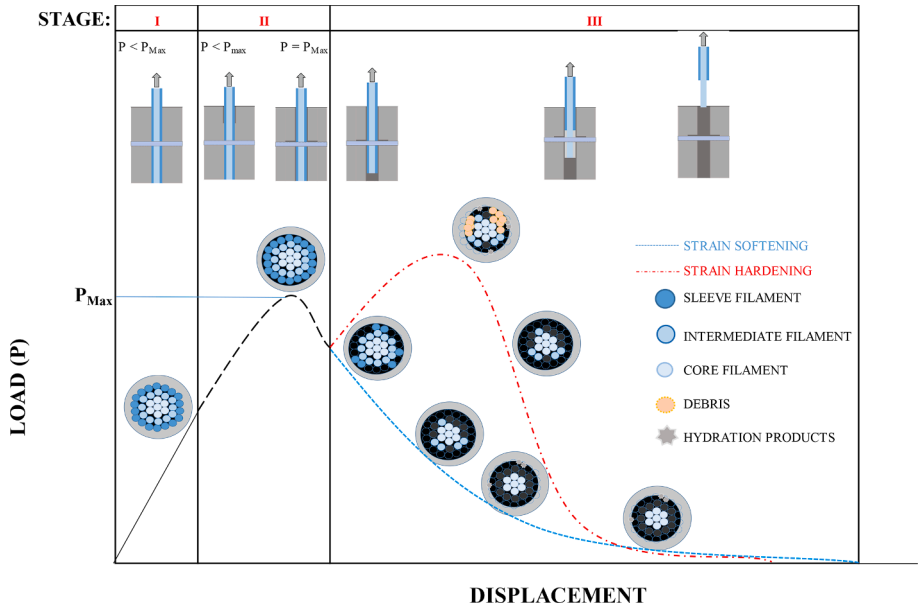

Fig. 18. A typical representation of the load-slip curve for a DSPOT and representation of the yarn degradation.

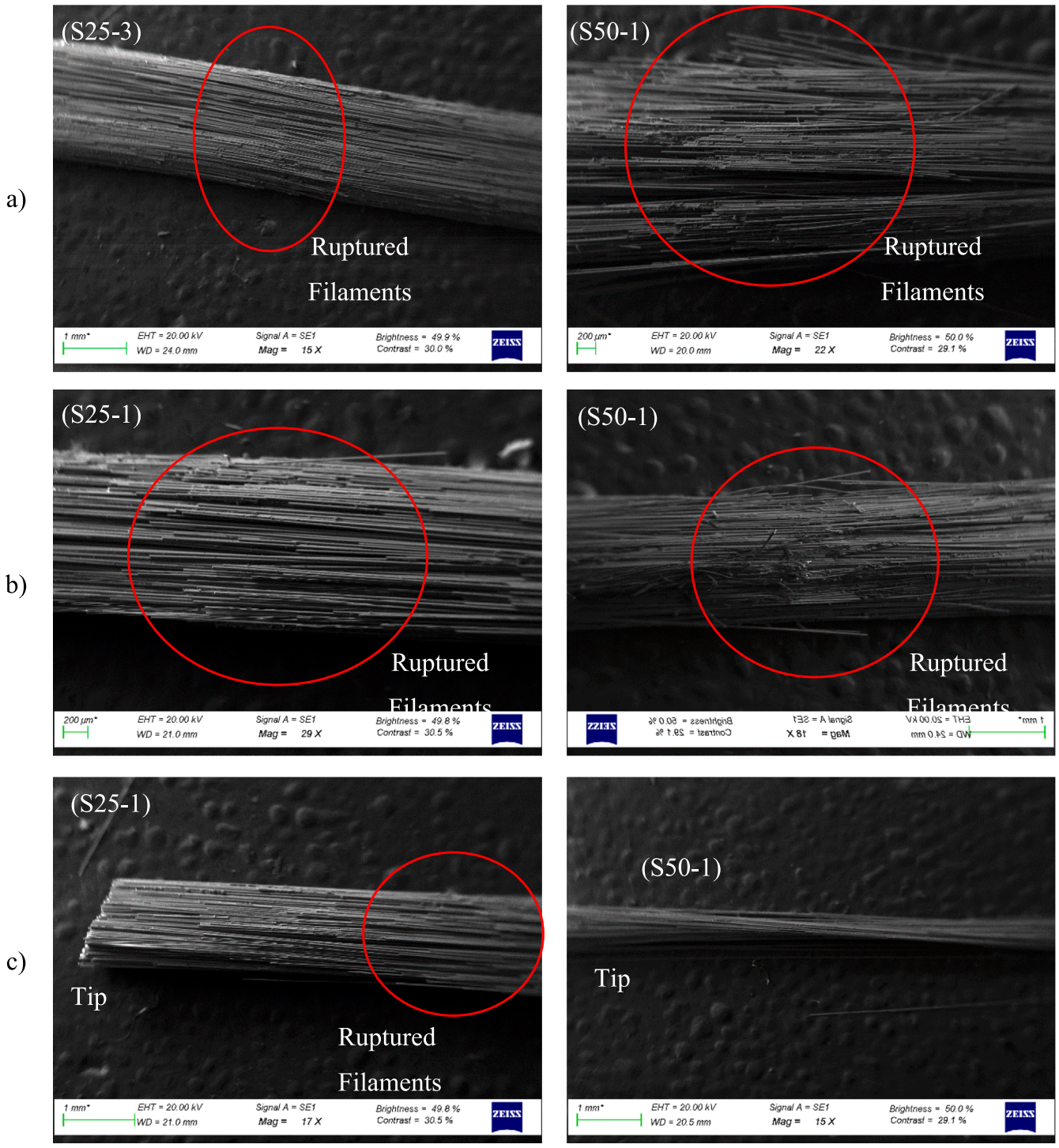

Fig. 19. SEM images showing the damage and slip occurring during yarn pull-out. (a) SEM images close to the extraction point. (b) SEM images at half the extracted length. (c) SEM images of the yarn-end.

prevalent in uncoated or surface-coated textiles (but that are not fully impregnated by the coating medium) since fully impregnated fibres do not exhibit telescopic failure to the same degree as a coated textile and are more likely to rupture. In other words, textiles that fail through telescopic failure may show signs of a congested bottleneck mechanism that enhances its resistance during pull-out. Thus, the congested bottleneck is shown to be another mechanism that is activated during the pull-out process.

4. Conclusions

This work was undertaken to research the impact of the damage done to a single yarn during the pull-out process. Imaging technology, in the form of SEM imaging and CT-scans, was used to investigate the post-pull-out damage on the yarn that is pulled out and the matrix from which the yarn is pulled. Telescopic failure was noted to occur, and the following mechanisms were identified to contribute to the failure mode based on literature and the experimental investigation in this study:

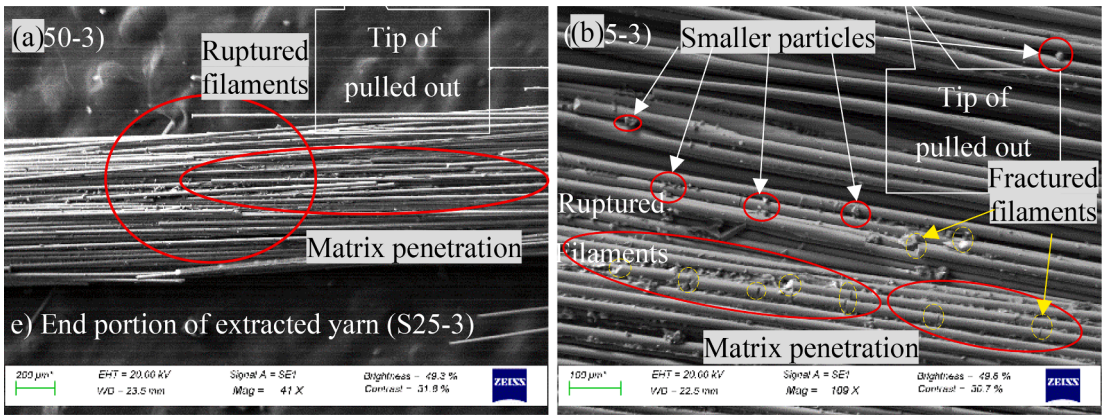

Fig. 20. SEM imaging of smaller particles penetrating the layers of the warp yarns for S25-3. (a) The presence of matrix penetration and ruptured filaments. (b) Small particles and fractured filaments.

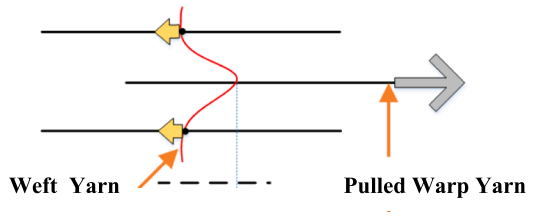

Fig. 21. The anchoring mechanism of weft yarns during the pull-out of warp yarns [53].

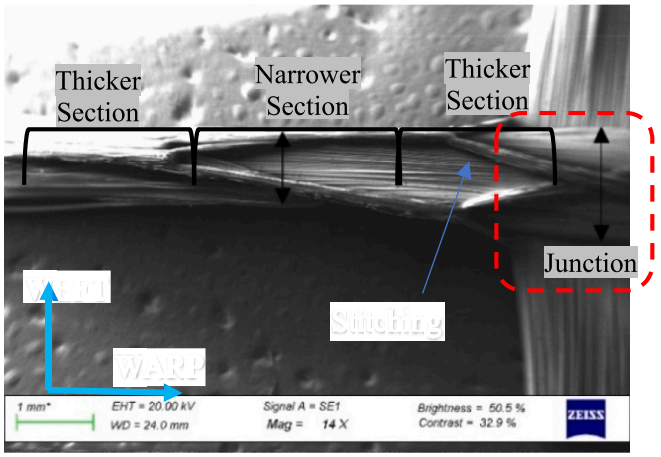

Fig. 22. SEM imaging displays the varying width of the warp yarn used in this study along its length before being embedded in a cement-based matrix.

1. The presence of hydration products and nanoparticles infiltrate the yarn and generate interlocking joints as suggested in literature;
2. The warp-weft junctions cause resistance against pull-out by anchoring the warp yarn as has been noted in literature;
3. At low levels of embedment (25 and 30 mm), pull-out with minor levels of telescopic failure dominates the failure mechanism. The telescopic mechanism is more dominant at longer embedment lengths (40 and 50 mm).
4. Beyond a 60 mm embedment length rupturing is seen to be the main failure mechanism. This is argued to result from the increase in surface area with an increase in length. That is, as the length increases, so does the frictional resistance. Hence, at an embedment length greater than 60 mm the frictional resistance is greater than the capacity of the filaments and rupturing ensues;

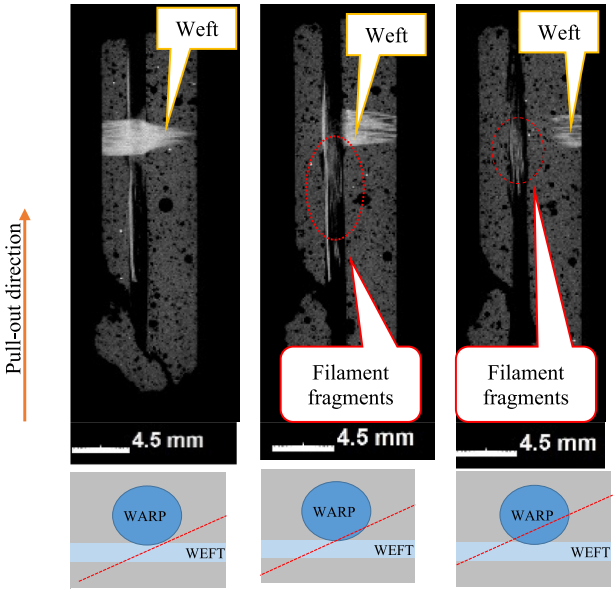

Fig. 23. The bottleneck effect of the yarn junction for an embedment length of 25 mm. The red line denotes the section of the CT-scan being shown. (For interpretation of the references to colour in this figure legend, the reader is referred to the web version of this article.)

5. A general pull-out behaviour model is developed (Figure 4.18). This model takes into consideration the effect of the length and the filament degradation. Additionally, this model set out to describe the effect that the debris has on the behaviour in terms of strain-hardening and softening;
6. The yarn junction also generates a bottleneck scenario which increases the pull-out resistance as congestion of particles and filaments accumulate at the junction as seen by this investigation. The bottleneck effect, and associated congestion, is argued to be present in textile's that exhibit telescopic failure. Further studies on its presence with epoxy-impregnated textiles would be beneficial.

The last mechanism related to bottlenecking has not been discussed in literature to date and provides a means of explaining the presence of secondary loading peaks during the pull-out process. The impact of the debris in the system adds value as it can potentially increase the resistance of the yarn during pull-out.

Furthermore, this means that more research, focusing on the undulating geometry, can provide insights on how to increase the capacity of

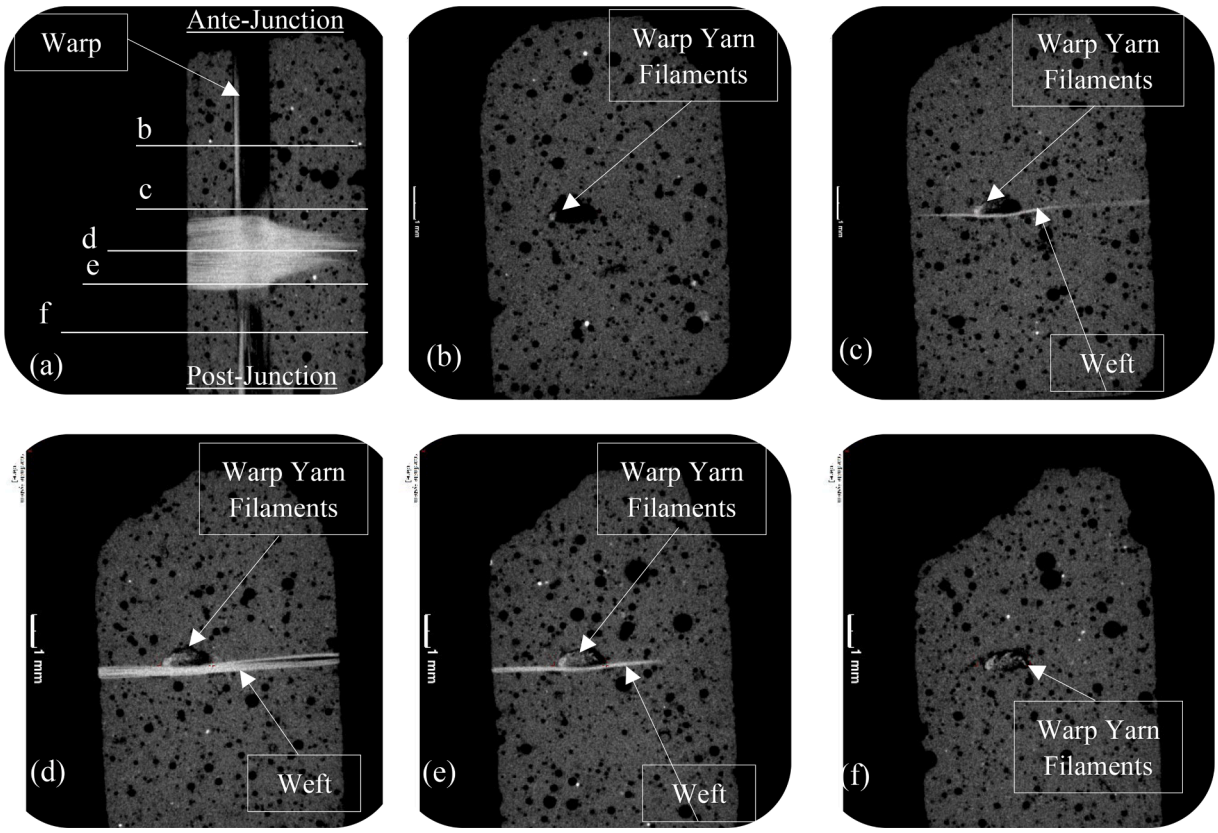

Fig. 24. The bottleneck effect of the yarn junction for an embedment length of 25 mm viewed from the top to the bottom of a warp-weft yarn connection: a) the location of the cross-section, b) away from the weft yarn, c) at the start of the weft yarn (ante-junction), d) middle section of the weft yarn, e) bottom of the weft yarn (post-junction), and f) away from the weft yarn.

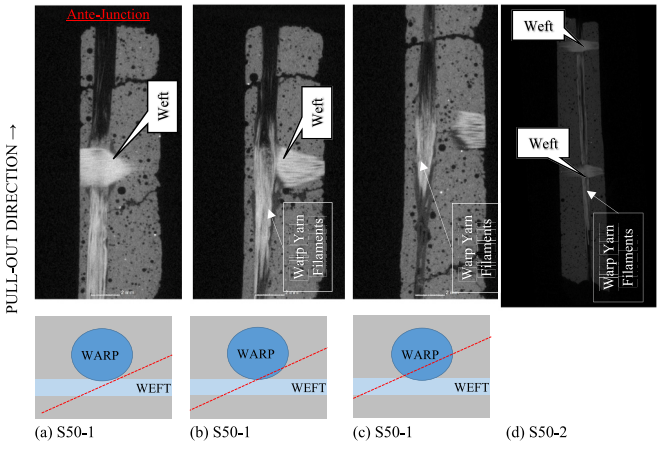

Fig. 25. The bottleneck effect of the weft-warp yarn connection for an embedment length of 50 mm. The progressive slides through the junction for S50-1 is shown in (a) to (c). Specimen S50-2 highlights the filemant fragments noted at two weft-warp junctions. The red line denotes the section of the CT-scan being shown. (For interpretation of the references to colour in this figure legend, the reader is referred to the web version of this article.)

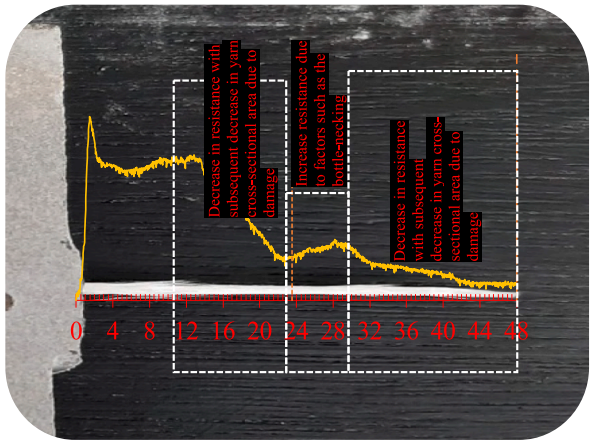

Fig. 26. Indication of the yarn resistance decreasing with the decrease in yarn cross-sectional area for S50-1. The load versus displacement plot for the associated sample is merged with an image of the yarn post-pull-out.

TRC after cracking. This would include adjusting the stitching and spacing of junctions to establish the extent of influence the bottleneck mechanism has. Moreover, as the mechanical interlock may be increased by the adding finer materials (SCMs or sand) to the coating, it is worth studying the extent of this enhancing on the congestion of the bottleneck mechanism. Additional research is recommended on this mechanism as only one textile, a surface-coated AR-glass textile, was tested.

CRediT authorship contribution statement

V.J.F. Alexandre: Writing – review & editing, Writing – original draft, Visualization, Validation, Resources, Methodology, Investigation, Formal analysis, Data curation, Conceptualization. **W.P. Boshoff:** Conceptualization, Methodology, Validation, Writing – review & editing, Supervision. **R. Combrinck:** Writing – review & editing, Visualization, Validation, Supervision, Resources, Project administration, Methodology, Investigation, Conceptualization.

Declaration of Competing Interest

The authors declare that they have no known competing financial interests or personal relationships that could have appeared to influence the work reported in this paper.

Data availability

Data will be made available on request.

Acknowledgements

This work is based on the research supported in part by the National Research Foundation of South Africa via the Thuthuka and Thrip funding instruments. Any opinion, findings and conclusions or recommendation expressed in this material is that of the author(s) and the NRF does not accept any liability on this regard. The support of Pretoria Portland Cement (PPC) and Chryso South Africa is also gratefully acknowledged.

References

[1] M.C. Rampini, G. Zani, M. Colombo, M. di Prisco, Mechanical behaviour of TRC composites: experimental and analytical approaches, Appl. Sci. 9 (2019) 1492, https://doi.org/10.3390/app9071492.
[2] C. Soranakom, B. Mobasher, Geometrical and mechanical aspects of fabric bonding and pullout in cement composites, Materials and Structures/Materiaux et, Constructions 42 (2009) 765–777, https://doi.org/10.1617/s11527-008-9422-6.
[3] T. D'Antino, C. Papanicolaou, Mechanical characterization of textile reinforced inorganic-matrix composites, Compos. B Eng. 127 (2017) 78–91, https://doi.org/10.1016/j.compositesb.2017.02.034.
[4] R. Contamine, A.S. Larbi, P. Hamelin, L.S. Bohr, U. Claude, B. Lyon, Tensile Identification of Textile Reinforcement Concrete Behaviour, in: W. Brameshuber (Ed.), International RILEM Conference on Material Science, RILEM Publications SARL, 2010, pp. 105–110.
[5] Y. Du, M. Zhang, F. Zhou, D. Zhu, Experimental study on basalt textile reinforced concrete under uniaxial tensile loading, Constr. Build. Mater. 138 (2017) 88–100, https://doi.org/10.1016/j.conbuildmat.2017.01.083.
[6] N. Williams Portal, I. Fernandez Perez, L. Nyholm Thrane, K. Lundgren, Pull-out of textile reinforcement in concrete, Constr. Build. Mater. 71 (2014) 63–71, https://doi.org/10.1016/j.conbuildmat.2014.08.014.
[7] C. Signorini, A. Sola, A. Nobili, C. Siligardi, Lime-cement textile reinforced mortar (TRM) with modified interphase, J. Appl. Biomater. Funct. Mater. 17 (2019), https://doi.org/10.1177/2280800019827823.
[8] M. Scheurer, T. Gries, Comparative evaluation of textiles for use in textile reinforced concrete, Mater. Today:. Proc. (2023), https://doi.org/10.1016/j.matpr.2023.03.477.
[9] A. Aveston, G.A. Cooper, A. Kelly, Single and Multiple Fracture, in: The Properties of Fibre Composites, IPC Science and Technology Press, London, 1971, pp. 15–24.
[10] J. Aveston, A. Kelly, Theory of multiple fracture of fibrous composites, J. Mater. Sci. 8 (1973) 352–362, https://doi.org/10.1007/BF00550155.
[11] R. Barhum, V. Mechtcherine, Effect of short, dispersed glass and carbon fibres on the behaviour of textile-reinforced concrete under tensile loading, Eng. Fract. Mech. 92 (2012) 56–71, https://doi.org/10.1016/j.engfracmech.2012.06.001.
[12] A. Peled, A. Bentur, B. Mobasher, Textile Reinforced Concrete, CRC Press, 2017.
[13] B. Banholzer, Bond of a strand in a cementitious matrix, Mater. Struct. 39 (2006) 1015–1028, https://doi.org/10.1617/s11527-006-9115-y.
[14] E. Lorenz, R. Ortlepp, Bond Behavior of Textile Reinforcements - Development of a Pull-Out Test and Modeling of the Respective Bond versus Slip Relation, (n.d.) 479–486.
[15] J. Wagner, M. Curbach, Bond Fatigue of TRC with Epoxy Impregnated Carbon Textiles, Appl. Sci. 9 (2019) 1980, https://doi.org/10.3390/app9101980.
[16] S. Xu, M. Krüger, H. Reinhardt, J. Ožbolt, Bond Characteristics of Carbon, Alkali Resistant Glass, and Aramid Textiles in Mortar, J. Mater. Civ. Eng. 16 (2004) 356–364, https://doi.org/10.1061/(ASCE)0899-1561(2004)16:4(356).
[17] S. Xu, H. Li, Bond properties and experimental methods of textile reinforced concrete, Journal of Wuhan University of Technology-Mater, Sci. Ed. 22 (2007) 529–532, https://doi.org/10.1007/s11595-006-3529-9.
[18] A. Peled, Strain Hardening Behaviour of Textile Reinforced Concrete (TRC), in: R. D. Toledo Filho, F.A. Silva, E.A.B. Koenders, E.M.R. Fairbairn (Eds.), 2nd International RILEM Conference on STrain Hardening Cementitious Composites (SHCC2-Rio), RILEM Publications SARL, 2011: pp. 45–52.
[19] A. Peled, E. Zaguri, G. Marom, Bonding characteristics of multifilament polymer yarns and cement matrices, Compos. A Appl. Sci. Manuf. 39 (2008) 930–939, https://doi.org/10.1016/j.compositesa.2008.03.012.
[20] S. Sueki, C. Soranakom, B. Mobasher, A. Peled, Pullout-Slip Response of Fabrics Embedded in a Cement Paste Matrix, J. Mater. Civ. Eng. 19 (2007) 718–727, https://doi.org/10.1061/(ASCE)0899-1561(2007)19:9(718).
[21] A. Peled, S. Sueki, B. Mobasher, Bonding in fabric–cement systems: Effects of fabrication methods, Cem. Concr. Res. 36 (2006) 1661–1671, https://doi.org/10.1016/j.cemconres.2006.05.009.
[22] A. Peled, B. Mobasher, S. Sueki, A comparison of processing technologies for the manufacture of textile cement-base composites, in: International RILEM Symposium on Concrete Science and Engineering: A Tribute to Arnon Bentur, RILEM Publications SARL, 2004: pp. 187–202. https://doi.org/10.1617/2912143586.017.
[23] J. Jiang, C. Jiang, B. Li, P. Feng, Bond behavior of basalt textile meshes in ultra-high ductility cementitious composites, Compos. B Eng. 174 (2019), 107022, https://doi.org/10.1016/j.compositesb.2019.107022.
[24] H. Aljewifi, X.B. Zhang, J. Li, Analysis on Pull-Out Behaviour of Continuous Multi-Filament Glass Yarns Embedded in Cementitious Matrix By Using a Developed Model, in: W. Brameshuber (Ed.), 11th International Symposium on Ferrocement and Textile Reinforced Concrete 3rd ICTRC ANALYSIS, RILEM Publications SARL, Bagneux, 2015.
[25] A. Aljewifi, B. Fiorio, J. Gallias, Pull-out behaviour of a glass multi-filaments yarn embedded in a cementitious matrix, in: N. Bićanić, R. de Borst, H. Mang, G. Meschke (Eds.), Computational Modelling of Concrete Structures, CRC Press, 2010, pp. 77–86.
[26] O. Homoro, M. Michel, T.N. Baranger, Pull-out response of glass yarn from ettringite matrix: Effect of pre-impregnation and embedded length, Compos. Sci. Technol. 170 (2019) 174–182, https://doi.org/10.1016/j.compscitech.2018.11.045.
[27] X.B. Zhang, H. Aljewifi, J. Li, Failure Mechanism Investigation of Continuous Fibre Reinforced Cementitious Composites by Pull-out Behaviour Analysis, Procedia, Mater. Sci. 3 (2014) 1377–1382, https://doi.org/10.1016/j.mspro.2014.06.222.
[28] C. Signorini, A. Sola, A. Nobili, Hierarchical composite coating for enhancing the tensile behaviour of textile-reinforced mortar (TRM), Cem. Concr. Compos. 140 (2023), 105082, https://doi.org/10.1016/j.cemconcomp.2023.105082.
[29] C. Soranakom, B. Mobasher, Modeling of tension stiffening in reinforced cement composites: Part I, Theoretical modeling, Materials and Structures/Materiaux et Constructions. 43 (2010) 1217–1230, https://doi.org/10.1617/s11527-010-9594-8.
[30] C. Soranakom, B. Mobasher, Modeling of tension stiffening in reinforced cement composites: Part II, Simulations versus experimental results, Materials and Structures/Materiaux et Constructions. 43 (2010) 1231–1243, https://doi.org/10.1617/s11527-010-9593-9.
[31] A. Peled, A. Bentur, Quantitative Description of the Pull-Out Behavior of Crimped Yarns from Cement Matrix, J. Mater. Civ. Eng. 15 (2003) 537–544, https://doi.org/10.1061/(ASCE)0899-1561(2003)15:6(537).
[32] M. Butler, V. Mechtcherine, S. Hempel, Durability of textile reinforced concrete made with AR glass fibre: effect of the matrix composition, Mater. Struct. 43 (2010) 1351–1368, https://doi.org/10.1617/s11527-010-9586-8.
[33] D. Dvorkin, A. Peled, Effect of reinforcement with carbon fabrics impregnated with nanoparticles on the tensile behavior of cement-based composites, Cem. Concr. Res. 85 (2016) 28–38, https://doi.org/10.1016/j.cemconres.2016.03.008.
[34] Z. Cohen, A. Peled, Controlled telescopic reinforcement system of fabric–cement composites — Durability concerns, Cem. Concr. Res. 40 (2010) 1495–1506, https://doi.org/10.1016/j.cemconres.2010.06.003.
[35] Z. Cohen, A. Peled, Effect of nanofillers and production methods to control the interfacial characteristics of glass bundles in textile fabric cement-based composites, Compos. A Appl. Sci. Manuf. 43 (2012) 962–972, https://doi.org/10.1016/j.compositesa.2012.01.022.
[36] M. Krüger, H.-W. Reinhardt, M. Fichtlscherer, Bond behaviour of textile reinforcement in reinforced and prestressed concrete, Otto-Graf-Journal. 12 (2001) 33–50.
[37] S. Gopinath, R. Gettu, N.R. Iyer, Influence of prestressing the textile on the tensile behaviour of textile reinforced concrete, Mater. Struct. 51 (2018) 64, https://doi.org/10.1617/s11527-018-1194-z.
[38] R. Kleicke, J. Hausding, E. Lorenz, R. Ortlepp, Research regarding the use of Stitch-bonded and Leno woven non Crimp Fabrics Reinforcements in Textile Reinforced Concrete, in: W. Brameshuber (Ed.), International RILEM Conference on Material Science, RILEM Publications SARL, 2010, pp. 45–55.
[39] A. Peled, A. Bentur, Reinforcement of cementitious matrices by warp knitted fabrics, Mater. Struct. 31 (8) (1998) 543–550.
[40] A. Peled, A. Bentur, Fabric structure and its reinforcing efficiency in textile reinforced cement composites, Compos. A Appl. Sci. Manuf. 34 (2003) 107–118, https://doi.org/10.1016/S1359-835X(03)00003-4.
[41] C.G. Papanicolaou, I.C. Papantoniou, Mechanical Behavior of Textile Reinforced Concrete (TRC) / Concrete Composite Elements, J. Adv. Concr. Technol. 8 (2010) 35–47, https://doi.org/10.3151/jact.8.35.
[42] C. Kulas, Actual applications and potential of textile-reinforced concrete, in: 17th International Congress of the GRCA, Dubai, United Arab Emirates, 2015: pp. 1–11.
[43] A.E. Naaman, Thin TRC products, in: Textile Fibre Composites in Civil Engineering, Elsevier, 2016, pp. 413–439.
[44] J. Hegger, S. Voss, Investigations on the bearing behaviour and application potential of textile reinforced concrete, Eng. Struct. 30 (2008) 2050–2056, https://doi.org/10.1016/j.engstruct.2008.01.006.
[45] G. Perry, G. Dittel, T. Gries, Y. Goldfeld, Mutual Effect of Textile Binding and Coating on the Structural Performance of TRC Beams, J. Mater. Civ. Eng. 32 (2020), https://doi.org/10.1061/(ASCE)MT.1943-5533.0003331.
[46] T. Quadflieg, O. Stolyarov, T. Gries, Influence of the fabric construction parameters and roving type on the tensile property retention of high-performance rovings in warp-knitted reinforced fabrics and cement-based composites, J. Ind. Text. 47 (2017) 453–471, https://doi.org/10.1177/1528083716652831.

[47] O. Weichold, Preparation and properties of hybrid cement-in-polymer coatings used for the improvement of fiber-matrix adhesion in textile reinforced concrete, J. Appl. Polym. Sci. 116 (2010) 3303–3309, https://doi.org/10.1002/app.31815.
[48] D. Zhu, X. Bai, Q. Yao, M.Z. Rahman, X. Li, T. Yang, S. Guo, Effects of volume fraction and surface coating of textile yarns on the tensile performance of AR-glass textile reinforced concrete, J. Build. Eng.. 71 (2023), 106420, https://doi.org/10.1016/j.jobe.2023.106420.
[49] C. Cherif, Textile Materials for Lightweight Constructions, Springer Berlin Heidelberg, Berlin, Heidelberg, 2016, 10.1007/978-3-662-46341-3.
[50] J. You, T. Kim, J. Park, S. Hong, S. Park, Adhesion performance according to lateral reinforcement method of textile, world academy of science, engineering and technology, Int. J. Civil, Environ., Struct., Constr. Arch. Eng. 11 (2017) 454–457.
[51] O.A. Cevallos, R.S. Olivito, Effects of fabric parameters on the tensile behaviour of sustainable cementitious composites, Compos. B Eng. 69 (2015) 256–266, https://doi.org/10.1016/j.compositesb.2014.10.004.
[52] M.K. Dolatabadi, S. Janetzko, T. Gries, Geometrical and mechanical properties of a non-crimp fabric applicable for textile reinforced concrete, J. Textile Inst. 105 (2014) 711–716, https://doi.org/10.1080/00405000.2013.844908.
[53] A. Peled, A. Bentur, D. Yankelevsky, Effects of Woven Fabric Geometry on the Bonding Performance of Cementitious Composites Mechanical Performance, Adv. Cem. Bas. Mat. 7 (1) (1998) 20–27.
[54] C. Scheffler, S.L. Gao, R. Plonka, E. Mäder, S. Hempel, M. Butler, V. Mechtcherine, Interphase modification of alkali-resistant glass fibres and carbon fibres for textile reinforced concrete I: Fibre properties and durability, Compos. Sci. Technol. 69 (2009) 531–538, https://doi.org/10.1016/j.compscitech.2008.11.027.
[55] K.B. Goliath, D.C.T. Cardoso, F. de A. Silva, Bearing behavior of Carbon-Textile-Reinforced Concrete Beams, Carbon-Und Textilebetontage. (2020) 42–47.
[56] H. Fataar, R. Combrinck, W.P. Boshoff, An experimental study on the fatigue failure of steel fibre reinforced concrete at a single fibre level, Constr. Build. Mater. 299 (2021), 123869, https://doi.org/10.1016/j.conbuildmat.2021.123869.
[57] P.D. Nieuwoudt, A.J. Babafemi, W.P. Boshoff, The response of cracked steel fibre reinforced concrete under various sustained stress levels on both the macro and single fibre level, Constr. Build. Mater. 156 (2017) 828–843, https://doi.org/10.1016/j.conbuildmat.2017.09.022.
[58] S.L. Gao, E. Mäder, R. Plonka, Coatings for glass fibers in a cementitious matrix, Acta Mater. 52 (2004) 4745–4755, https://doi.org/10.1016/j.actamat.2004.06.028.
[59] W. Wu, X. He, W. Yang, M.S. Alam, B. Wei, J. He, Degradation factors and microstructure degradation characteristics of B/GFRP bars in harsh environment: A review, Constr. Build. Mater. 366 (2023), 130246, https://doi.org/10.1016/j.conbuildmat.2022.130246.
[60] F. Bompadre, J. Donnini, Surface Modification of Glass Textile for the Reinforcement of a Cement-Based Composite: A Review, Appl. Sci. 11 (2021) 2028, https://doi.org/10.3390/app11052028.
[61] A. Spelter, S. Bergmann, J. Bielak, J. Hegger, Long-term durability of carbon-reinforced concrete: an overview and experimental investigations, Appl. Sci. 9 (2019) 1651, https://doi.org/10.3390/app9081651.
[62] J. Tu, H. Xie, K. Gao, Prediction of the long-term performance and durability of GFRP bars under the combined effect of a sustained load and severe environments, Materials. 13 (2020) 2341, https://doi.org/10.3390/ma13102341.
[63] V. Fraas, Technical Datasheet: SITgrid027, (2017). https://solutions-in-textile.com/produkte/verstaerkung-und-instandsetzung.
[64] Mapei, Dynamon SP1, (2020).
[65] RILEM Technical Committee 232-TDT, Recommendation of RILEM TC 232-TDT: test methods and design of textile reinforced concrete, Mater Struct. 49 (2016) 4923–4927. https://doi.org/10.1617/s11527-016-0839-z.
[66] M. Butler, V. Mechtcherine, S. Hempel, Experimental investigations on the durability of fibre – matrix interfaces in textile-reinforced concrete, Cem. Concr. Compos. 31 (2009) 221–231, https://doi.org/10.1016/j.cemconcomp.2009.02.005.
[67] E. Lorenz, R. Ortlepp, Basic research on the anchorage of textile reinforcement in cementitious matrix, (2009).
[68] A. Dalalbashi, B. Ghiassi, D.V. Oliveira, A. Freitas, Effect of test setup on the fiber-to-mortar pull-out response in TRM composites: Experimental and analytical modeling, Compos. B Eng. 143 (2018) 250–268, https://doi.org/10.1016/j.compositesb.2018.02.010.
[69] S. Liu, P. Rawat, Z. Chen, S. Guo, C. Shi, D. Zhu, Pullout behaviors of single yarn and textile in cement matrix at elevated temperatures with varying loading speeds, Compos. B Eng. 199 (2020), 108251, https://doi.org/10.1016/j.compositesb.2020.108251.
[70] P. Valeri, M. Fernàndez Ruiz, A. Muttoni, Tensile response of textile reinforced concrete, Constr. Build. Mater. 258 (2020), 119517, https://doi.org/10.1016/j.conbuildmat.2020.119517.
[71] M.Y. Yardımcı, R. Tirosh, P. Larianovsky, M. Puterman, A. Bentur, Improving the bond characteristics of AR-glass strands by microstructure modification technique, Cem. Concr. Compos. 33 (2011) 124–130, https://doi.org/10.1016/j.cemconcomp.2010.09.005.
[72] H.W. Reinhardt, M. Krüger, C.U. Große, Concrete Prestressed with Textile Fabric, J. Adv. Concr. Technol. 1 (3) (2003) 231–239.
[73] R. Ortlepp, Efficient Adaptive Test Method for Textile Development Length in TRC, Adv. Civil Eng. 2018 (2018) 1–14, https://doi.org/10.1155/2018/4650102.
[74] B. Mobasher, A. Peled, J. Pahilajani, Pultrusion of Fabric Reinforced High FLy Ash Blended Cement Composites, in: M. di Prisco, R. Felicetti, G.A. Plizzari (Eds.), 6th International RILEM Symposium on Fibre-Reinforced Concretes (BEFIB'2004), RILEM Publications SARL, 2004, pp. 1473–1482.
[75] P. Preinstorfer, J. Kollegger, New insights into the splitting failure of textile-reinforced concrete, Compos. Struct. 243 (2020) 112–203, https://doi.org/10.1016/j.compstruct.2020.112203.